Be ITER-like wall at the JET tokamak under plasma

Plasma interaction with Be wall at the JET tokamak with the ITER-Like Wall

P. Tsavalas[a,b], A. Lagoyannis[c], K. Mergia[a*], K. Triantou[a], M Kokkoris[b], S Harissopulos[c], M. Rubel[d], P. Petersson[d] and JET Contributors[**]

[a] National Centre for Scientific Research "Demokritos", Institute of Nuclear and Radiological Science and Technology, Energy and Safety, 15310 Aghia Paraskevi, Athens, Greece

[b] National Technical University of Athens, Department of Physics, Zografou Campus, Athens, Greece

[c] National Centre for Scientific Research "Demokritos", Institute of Nuclear and Particle Physics, 15310 Aghia Paraskevi, Athens, Greece

[d] Department of Fusion Plasma Physics, Royal Institute of Technology (KTH), 100 44 Stockholm, Sweden

***See the author list in: X. Litaudon et al., Nuclear Fusion Special issue: 26th Fusion Energy Conference (Kyoto, Japan, October 2016)*

[*]Corresponding author: K. Mergia, tel. +30 2106503706, email: kmergia@ipta.demokritos.gr

Abstract

The JET tokamak is operated with beryllium and tungsten plasma-facing components to prepare for the exploitation of ITER. To determine beryllium erosion and migration in JET a set of markers were installed. Specimens from different beryllium marker tiles of the main wall of the ITER-like wall JET tokamak from the first and the second D-D campaign were analyzed with nuclear reaction analysis, X-ray fluorescence spectroscopy, scanning electron microscopy and X-ray diffraction. Emphasis was on the determination of carbon plasma impurities deposited on beryllium surfaces. The $^{12}C(d,p_0)^{13}C$ reaction was used to quantify carbon deposition and to determine depth profiles. Carbon quantities are low, varying from 0.35×10^{17} to 11.8×10^{17} at/cm^2 in the deposition depth from 0.4 to 6.7 μm. In addition, oxygen, titanium, chromium, manganese, iron, nickel and tungsten were detected in all samples. Nickel is the metallic element with the highest deposition originating from the Inconel parts inside the JET main chamber. XRD shows the formation of BeNi in most specimens.

Keywords: *plasma, JET tokamak, beryllium, erosion-deposition, ITER-Like Wall, nuclear reaction analysis*

PACS: 52.40.Hf

1. Introduction

The Joint European Torus (JET) tokamak, the largest controlled fusion device with magnetic confinement in the world, investigates the potential of fusion power as a future energy source [1]. Its main scientific mission is to develop plasma operation scenarios for a reactor-class machine such as ITER (International Thermonuclear Experimental Reactor). This includes also the performance test of plasma-facing materials (PFM) and components (PFC).

Fuel retention and material migration (erosion and deposition processes) are the main consequences of plasma impact on PFM. A comprehensive understanding of these mechanisms is crucial for the safe operation of a fusion reactor. To respond to ITER challenges, since 2011 JET is operated with the ITER-Like Wall (JET-ILW), i.e. the wall materials are such as suggested for ITER: beryllium in main chamber wall and tungsten in the divertor [2, 3]. Earlier, for over two decades, carbon was the main material of the JET wall (JET-C). High fuel inventory with carbon PFM was the main driving force for the change in JET wall to carry out a large-scale material test for ITER. Three ILW campaigns have been conducted: 2011-2012, 2013-2014 and 2015-2016. After each campaign a selection of wall tiles and wall probes [3] were retrieved. Until now, materials from the first two periods have been made available for ex-situ analyses. Ample set of results have already been reported on erosion [4, 5], fuel retention [6, 7, 8], melting [9] and material deposition [10, 11]. However, the quantification of carbon deposition on surfaces has been missing. The most efficient characterisation of PFC surfaces is carried by ion beam analysis (IBA) techniques. Unfortunately, the possibility of carbon determination with either a H^+ or a ^3He ion beam is truly difficult in the presence of significant amounts of beryllium. The aim of this work is to elaborate analytical approach towards carbon quantification on beryllium wall components from JET-ILW.

2. Experimental Samples and Experimental Details

The study was carried out for samples sectioned from several marker tiles [12] after two ILW campaigns. Samples from marker tiles: one from the Upper Dump Plate (UDP, 2B(C)2), two from the mid-plane of the Outer Poloidal Limiter (OPL, 4D14) and four from the mid-plane of the Inner Wall Guard Limiter (IGWL, 2XR10) of the ITER-like wall JET tokamak were analyzed.

The carbon content was examined by means of nuclear reaction analysis (NRA) using the $^{12}C(d,p_0)^{13}C$ reaction employing a 1.35 MeV deuteron beam. A silicon surface-barrier detector was placed at 170^o with

respect to the beam axis. A thin Kapton foil in front of the detector was employed in order to separate the proton from the alpha peaks [13]. The experiment was carried out under high vacuum (10^{-7} mbar).

The depth profile of carbon was assessed using the nuclear reactions: $^{12}C(d,p_0)^{13}C$ and $^{9}Be(d,p_0)^{10}Be$. For the $^{12}C(d,p_0)^{13}C$ reaction, the cross section evaluated by Sigmacalc [14] was used. The cross-section of the $^{9}Be(d,p_0)^{10}Be$ reaction was measured at various angles and energies for the needs of the current work. The simulation of the experimental data was performed using the SIMNRA software package [15].

SEM measurements were carried out on a FEI Quanta Inspect SEM coupled with EDS. For the EDS analysis a voltage of 12.5 kV was used. In addition, the deposition of metallic elements and the formation of compounds are investigated by X-ray fluorescence spectroscopy (XRF) and X-ray diffraction (XRD), respectively. The XRF spectra were measured using the Amptek system with an Ag X-ray tube, a high voltage of 30 kV and a silicon drift detector [16]. A collimator of 1 mm diameter was used. Elements with Z>11 are detected with a detection limit in the order of ppm. Quantification was achieved using a NIST stainless steel 316 standard [17]. XRD measurements were carried out on a Bruker D8 spectrometer using Cu K_α radiation, a parallel beam stemming from a Göbbel mirror and VÄNTEC linear position-sensitive detector.

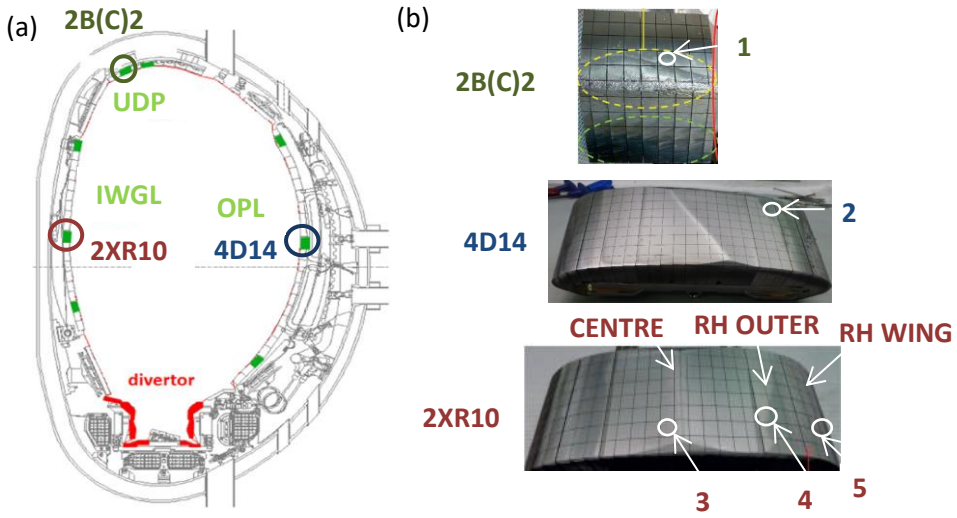

.Fig. 1. a) Poloidal cross-section of JET with marked location of samples and tile notation; the studied tiles are circled; b) limiter tiles with marked position of the studied samples.

Fig.1 depicts the position of the marker tiles in the tokamak and the position of the samples on the tiles. The description of the samples is given in Table 1. The initial composition of the samples was Be

(bulk)/Ni (2-3 μm)/Be(7-9 μm) where Ni was used as an interlayer in order to assess the erosion of the sample surface.

3. Results and Discussion

In NRA spectra the $^{12}C(d,p_0)^{13}C$ peak is present for all specimen under examination. As mentioned in the introduction, JET was operated in the past with carbon wall. In JET-ILW tungsten-coated carbon fibre composite (W/CFC) tiles are in the divertor and in some areas in the main chamber wall [2]. Spectroscopy data clearly prove that carbon fluxes have been strongly reduced (15-20 times) after the change of the wall, but not fully eliminated.

Fig.2 shows the NRA spectrum of the IWGL (76) sample which is a representative spectrum for all the samples. The peaks from the $^{9}Be(d,p_0)^{10}Be$, $^{9}Be(d,t)^{8}Be$ and $^{9}Be(d,a_0)^{7}Li$ reactions are clearly observed. On most of the samples, the oxygen peaks of $^{16}O(d,p_0)^{17}O$ and $^{16}O(d,p_1)^{17}O$ reactions were detected. The quantification of the oxygen can be achieved when the cross sections from these reactions become available. In addition, for OPL (120) and IWGL (76) samples the peak of the $^{2}H(d,p)^{3}H$ is well-defined.

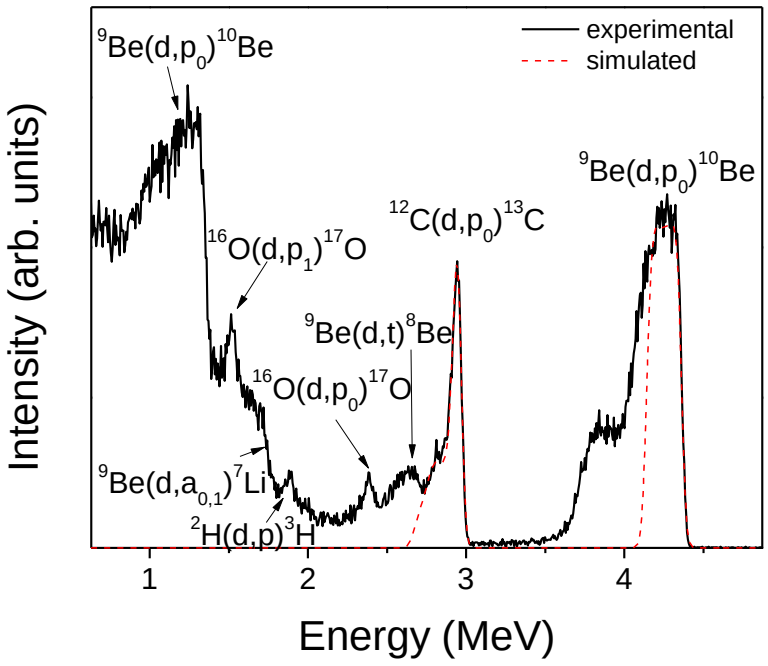

Fig. 2. Experimental (black-solid line) and simulated (red-dash line) spectrum of the IWGL (76) sample**.**

From the simulation (dotted line in Fig.2) of the NRA spectra, in the range of energy where the reactions $^{12}C(d,p_0)^{13}C$ and $^{9}Be(d,p_0)^{10}Be$ are detected, the carbon depth profile was determined. The peak on the left of the $C(d,p_0)$ peak, which corresponds to the $^{9}Be(d,t)^{8}Be$, reaction cannot be simulated due to the lack of the required cross section. The $Be(d,p_0)$ peak is simulated for energies larger than 1 MeV since for lower energies the cross sections are not available in the literature. The cross section of the $^{9}Be(d,p_0)^{10}Be$ reaction for energies in the range 1 to 2.2 MeV were measured for the aim of the current work. It is noted that the left profile of the $Be(d,p_0)$ peak is related with Be erosion and Be/Ni mixing, as it will be discussed below. The total density and the extent of the deposition layer with the presence of carbon are collected for all the samples in the last two columns of Table 1. There are differences in the carbon content between respective samples, but the most important is generally the small total content (maximum at 11.8×10^{17} at/cm^2) clearly reflecting low carbon fluxes during the ILW operation. It also indicates that the damage of the tungsten coatings on CFC has been limited.

The greatest amount of carbon (11.8×10^{17} at/cm^2) co-deposited in a layer of 6.7 μm has been measured on the surface of UDP (80). The lowest density (0.35×10^{17} at/cm^2) and significantly smaller amount (with corresponding layer thickness of 0.4 μm) has been detected on OPL (320). The lower carbon deposition on OPL during the 2nd campaign compared to the 1st one must be related with the enhanced erosion of the sample 320 from OPL during the 2nd campaign, as it will be discussed below. The low amount in the central part of the IWGL (174) is explained by the fact that the sample originates from the erosion zone.

Table 1. Total carbon density and the thickness of the carbon-containing layer.

Tokamak area	Tile no	Tile area	Campaign	Sample Code	C density (10^{17}at/cm^2)	C deposition thickness (μm)
DP	2B(C)2	Centre	1	**DP (80)**	11.8	6.7
OPL	4D14	W3 RH	1	**OPL (120)**	2.66	3
		W3 RH	2	**OPL (320)**	0.35	0.4
IWGL	2XR10	Centre	1	**IWGL (174)**	0.70	0.8
		RH outer	1	**IWGL (27)**	3.59	2.3
		RH outer	2	**IWGL (191)**	4.00	3.7
		RH wing	1	**IWGL (76)**	7.60	5.5

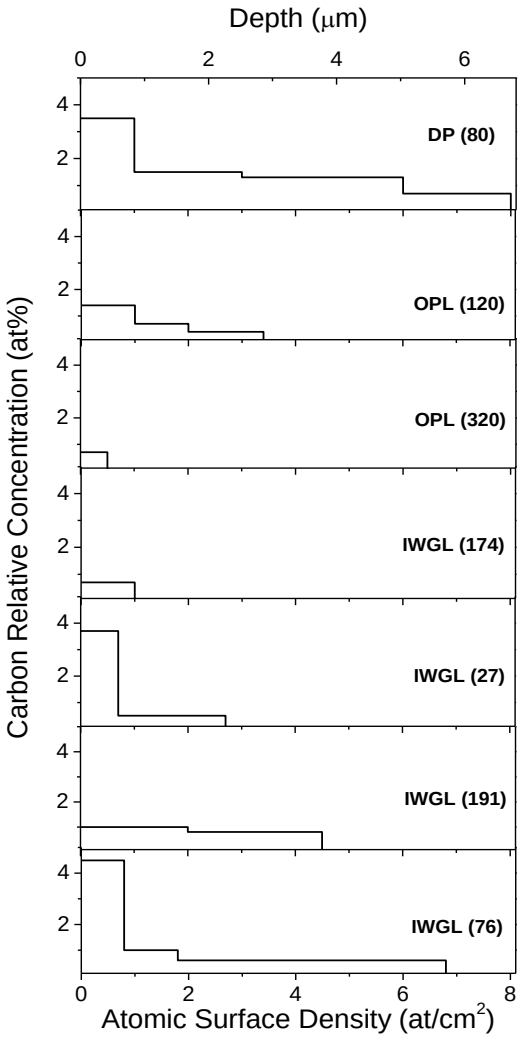

Fig. 3 Relative carbon content in at% plotted versus depth for the different areas of the JET tokamak for the ILW-1 and ILW-2.

The change of the carbon concentration (relative to beryllium) with depth in the deposition layer is depicted in Fig. 3. It is perceived that the concentration decreases as a function of depth in all the investigated samples and moreover the decrease is drastic at about 1 μm depth. The highest surface concentration (4.5 at%) was detected on the IWGL (76). A significant difference is observed in OPL and IWGL areas between the 1st and the 2nd campaign.

Fig.4 presents the NRA spectrum focused on the energy range of the $^{9}Be(d,p_0)^{10}Be$ reaction of the exposed samples to plasma compared to the reference (not exposed to plasma) one with composition Be (bulk)/Ni(2 μm)/Be(9 μm).

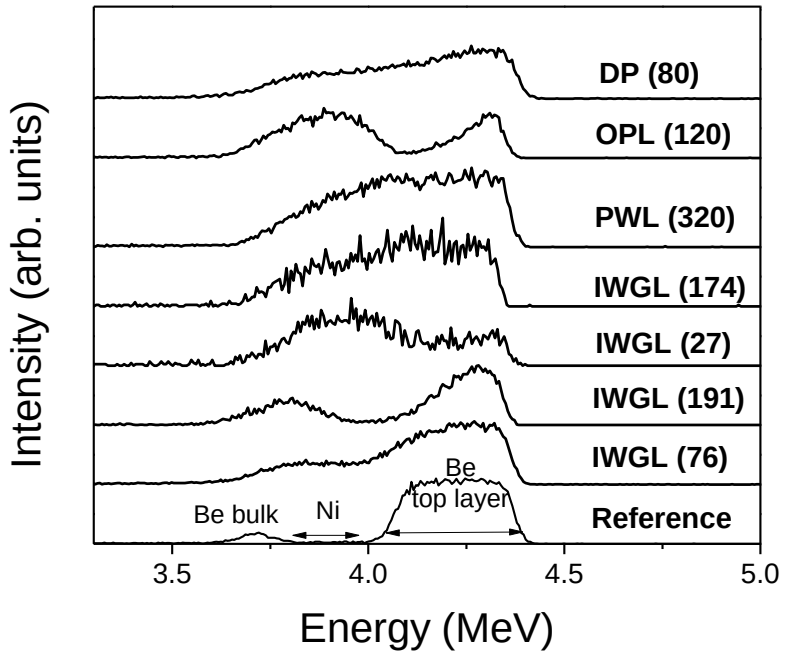

Fig. 4. Comparison of $^{9}Be(d,p_0)^{10}Be$ peak between the reference and the exposed to plasma samples.

In the reference sample the absence of the $^{9}Be(d,p_0)^{10}Be$ peak in the energy range 3.8 to 4 MeV (Fig. 4) is related with the presence of the Ni interlayer at a depth of about 9 μm. The small peak between 3.6 and 3.8 MeV corresponds to the Be bulk below the Ni interlayer. One observes that in OPL (320) and IWGL (174) the Ni interlayer is completely missing, thus these two areas have undergone enhanced erosion. In the OPL (120) and IWGL (191) samples the surface Be is thinner than in the reference sample, leading to the conclusion that these samples had suffered erosion which is less than 8 μm. The comparison with the reference sample when performed for the samples DP (80) and IWGL (76) shows that the Ni interlayer is mixed with the Be. On the other hand, in IWGL (191) the presence of the Ni interlayer is clearly indicated.

Nuclear reaction analyses with standard size beam were also performed on surfaces located inside the castellated grooves. The average carbon concentration in the castellated sides for the majority of the samples is 4×10^{17} at/cm^2. Higher concentration has been measured on two samples: IWGL (27) and DP (80). No significant differences have been observed between four sides of the castellated samples. The results indicate that the deuterium inventory inside the castellated grooves **[**18**]** is to a high extent related to the presence of carbon.

The XRF results are presented in Fig.5. It is noted that these results refer to elements with Z>11, thus the mentioned concentration does not take into account C and Be. Chromium (Cr), manganese (Mn), iron (Fe), nickel (Ni), titanium (Ti) and tungsten (W) were detected in all samples. It is noted that the peaks of Copper (Cu) and Zinc (Zn) are present in the spectra because of the beam collimator made from brass and their content in the samples, if any, cannot be quantified. However, EDS analysis does not show the presence of Cr and Zn. Cr, Mn, Fe, Ni and Ti come from the Inconel parts present in the JET main chamber, and in some samples (apart from OPL (320) and IWGL (174)) from the Ni interlayer. The presence of W is due to its migration from the JET divertor. All samples have similar nickel relative concentration apart from OPL (320) and IWGL (174) because in the last two samples the Ni interlayer has been eroded as concluded from the NRA data and discussed above. The strong erosion (>50 μm) of the center area of the 2X10 Tile is confirmed by the results of Ref. [10].

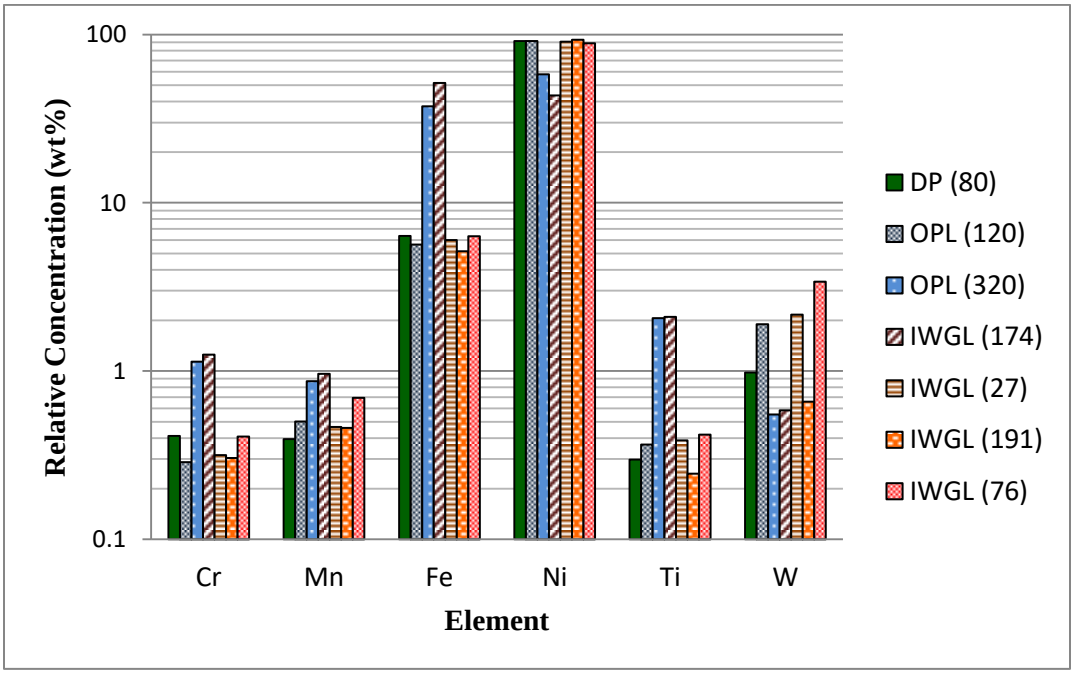

Fig. 5. XRF results of the analyzed samples. The concentration refers to elements with Z>11.

Fig.6 depicts the SEM images of some of the sample surfaces. The sample surfaces present quite different morphology. It is pointed out that white areas correspond to heavy elements whereas light elements are depicted gray. Intense deposition or erosion and re-deposition is observed on DP (80) in conjunction with

NRA spectrum (Fig.4). OPL (320), which has undergone enhanced erosion of more than 11 μm as revealed by NRA, presents deposition areas in the form of particles rich in Ni. In IWGL (27) the Ni interlayer (white area) is revealed through the partial erosion of the above Be layer (black area). OPL (120) sample (not shown) has been undergone erosion of its Be layer in the area towards the center of the tile. Prolonged beryllium structures are observed in sample IWGL (174) (not shown) which has been eroded for depths larger than 11 μm (Fig.4) in agreement with the results of ref. [11]. IWGL (76) (not shown) seems to have undergone melting.

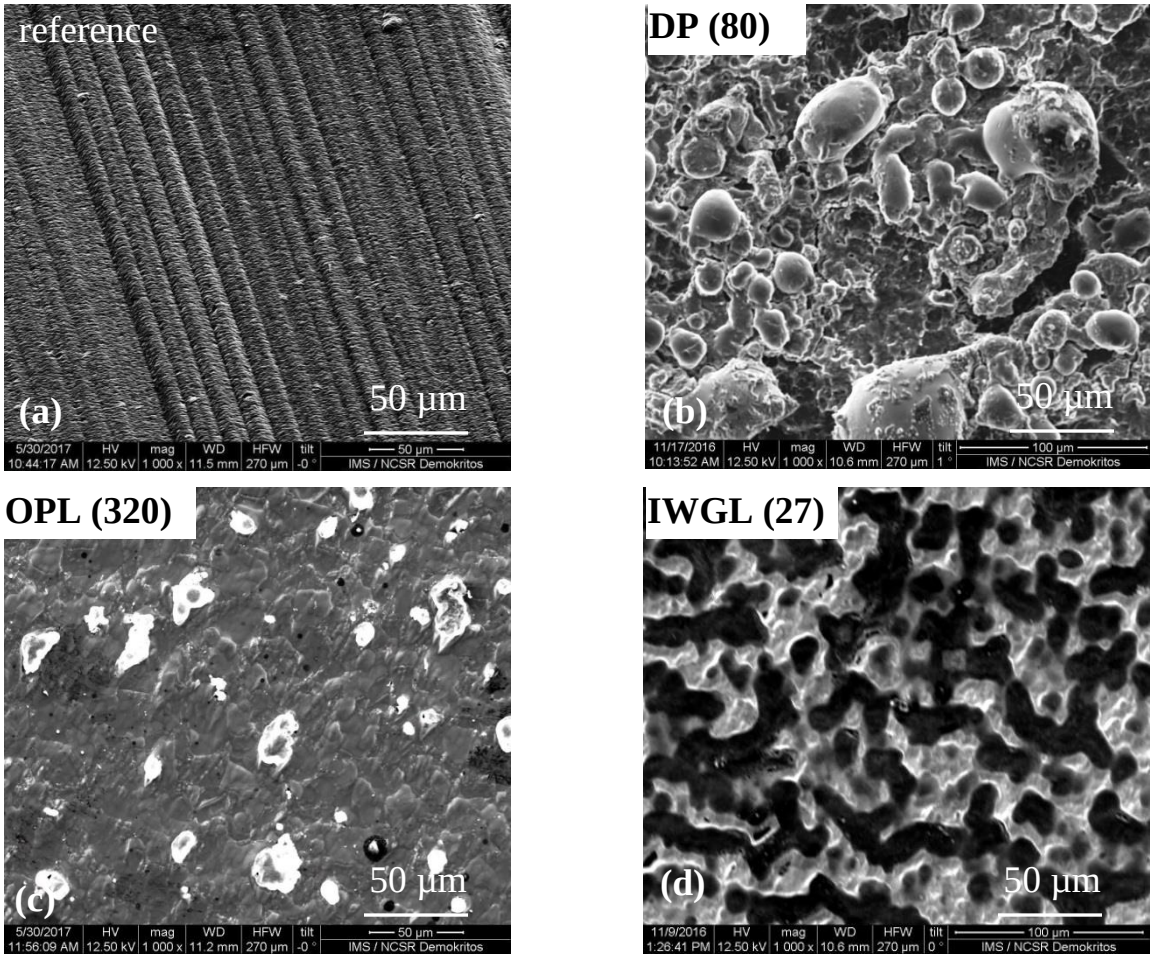

Fig. 6. SEM images of the sample surfaces.

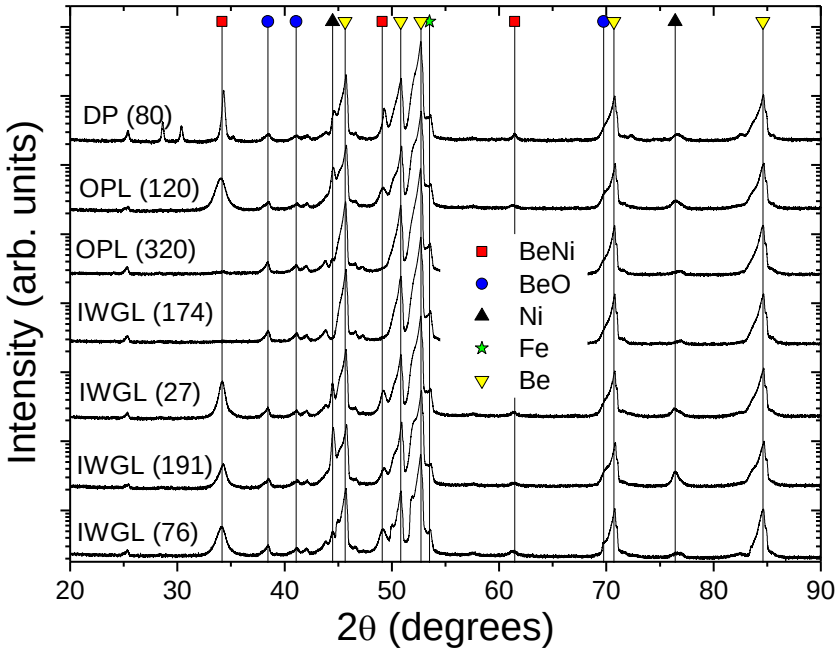

Fig. 7. XRD spectra of the samples and the detected phases.

XRD spectra (Fig. 7) show the formation of BeO in all samples. BeO is crystallized in the hexagonal system with Space Group 186. The oxidation of beryllium is a common phenomenon and the increase of the temperature enhances the oxidation [19]. Furthermore, the BeNi alloy and Ni are detected in all samples except for OPL (320) and IWGL (174). Furthermore, the absence of the Ni peak confirms its low concentration in these two samples, in agreement with the NRA and XRF results. BeNi is crystallized in the cubic system with Space Group 221.

4. Conclusions

Different samples from the beryllium limiter tiles retrieved after the first and the second campaign of the JET-ILW main chamber were investigated by a set of material research techniques. The most important contribution of this work for the characterisation of PFC is the quantification of carbon content in co-deposits. The results prove low C contents. No significant differences between samples from the ILW campaigns have been observed. Metals such as Cr, Mn, Fe, Ni, Ti and W are detected by XRF spectroscopy. The presence of Ti, Cr, Mn, Fe and Ni is mainly due to the erosion of the Inconel parts present in the main JET chamber, and partially from the Ni interlayer marker if the latter has not been

eroded. In the central part of the IWGL from the first campaign and in OPL from ILW-2 no Ni interlayer has been detected. This is attributed to the enhanced erosion of these areas of more than 10 μm. XRD demonstrates a significant result, that of the formation of BeNi intermetallic compound. In summary, these new results, especially on carbon content, complement previous data on fuel retention and wall erosion [4,6-8,10,18]. From these results in conjunction with previous findings emerges a complete picture regarding the modification of beryllium limiters under plasma impact in two JET-ILW campaigns.

Acknowledgments

This work was carried out within the EUROfusion Consortium and received funding from the EURATOM research and training programme 2014-2018 under grant agreement number No 633053. The views and opinions expressed herein do not necessarily reflect those of the European Commission.

References

[1] https://www.euro-fusion.org/jet/
[2] Matthews G F et al 2011 *Phys.Scr*. **T145** 014001 (6pp)
[3] Rubel M. et al 2013 *J. Nucl. Mater*. **438** S1204-S1207
[4] Baron-Wiechec A et al 2015 *J. Nucl. Mater.* **463** 157-161
[5] Krat S, Mayer M, Bykov I, Kungu C P, de Saint Aubin G, Widdowson A, Carvalho I S, JET contributors 2017 *Nucl. Mater. Energy* **11** 20-24
[6] Brezinsek S et al 2013 *Nucl. Fusion* **53** 083023 (13pp)
[7] Heinola K et al 2015 *J. Nucl. Mater.* **463** 961-965
[8] Heinola K et al 2016 *Phys. Scr*. **T167** 014075 (7pp)
[9] Matthews G F et al 2016 *Phys. Scr.* **T167** 014070 (7pp)
[10] Heinola K, Ayres C F, Baron-Wiechec A, Coad J P, Likonen J, Matthews G F, AWiddowson A and JET-EFDA Contributors 2014 *Phys. Scr*. **T159** 014013 (5pp)
[11] Pajuste E, Kizane G, Vitins A, Igaune I , Avotina L, Zarins R and JET contributors 2017 *J Nucl Mater and Energy* (*in press*)
[12] Lungu CP, Mustata I, Zaroschi V, Lungu A M, Anghel A, Chiru P, Rubel M, Coad P, Matthews G F and JET-EFDA contributors 2007 *Phys. Scr*. **T128** 157-161
[13] Lagogiannis A, Tsavalas P, Mergia K, Provatas G, Triantou K, Tsompopoulou E O, Rubel M, Petersson P, Widdowson A, Harissopulos S, Mertzimekis T 2017 *Nuclear Fusion* (in press)
[14] Gurbich A F 2016 *J. Nucl. Instr. Meth. B*. **371** 27-32
[15] Mayer M 1999 *AIP Conf. Proc*. **475** 541 – 544
[16] http://amptek.com/product/complete-xrf-experimenters-kit/
[17] NIST SRM 160b, https://www-s.nist.gov/srmors/view_cert.cfm?srm=160B
[18] Rubel M et al 2017 *Nucl. Fusion* **57** 066027 (7pp)
[19] Roth J, Doerner R, Baldwin M, Dittmar T, Xu H, Sugiyama K, Reinelt M, Linsmeier Ch, Oberkofler M 2013 *J. Nucl. Mater.* **438** S1044-S1047